



Agricultural drought over water-scarce Central Asia aggravated by internal climate variability

Received: 9 May 2022

Jie Jiang ¹ & Tianjun Zhou ^{1,2}

Accepted: 6 December 2022

Published online: 12 January 2023

Check for updates

A severe agricultural drought swept Central Asia in 2021, causing mass die-offs of crops and livestock. The anthropogenic contribution to declines in soil moisture in this region over recent decades has remained unclear. Here we show from analysis of large ensemble simulations that the aggravation of agricultural droughts over southern Central Asia since 1992 can be attributed to both anthropogenic forcing and internal variability associated with the Interdecadal Pacific Oscillation (IPO). Although the negative-to-positive phase transition of IPO before 1992 offset human-induced soil moisture decline, we find that the positive-to-negative phase transition thereafter has doubled the externally forced rate of drying in the early growing season. Human-induced soil moisture loss will probably be further aggravated in the following century due to warming, albeit with increasing precipitation, and our simulations project that this trend will not be counterbalanced by the IPO phase change. Instead, this internal variability could modulate drying rates in the near term with an amplitude of -2 ($+2$) standard deviation of the IPO trend projected to amplify (weaken) the externally forced decrease in surface soil moisture by nearly 75% (60%). The findings highlight the need for the interplay between anthropogenic forcing and the natural variability of the IPO to be considered by policymakers in this climate-sensitive region.

Central Asia suffered from an extreme agricultural drought in its early growing season in 2021. Crops withered due to insufficient water supplies, and thousands of sheep, cows and horses had died because of the lack of water and forage. The harsh drought of 2021 is not an independent event but a part of a drier trend over the past half century^{1–3}. Soil moisture has been used as an indicator of agricultural and ecological drought⁴. The loss of soil moisture has accelerated in recent decades, which has intensified desertification in this arid region and led to a more fragile ecosystem^{5–7}. For water resource-limited environments such as Central Asia, the reduction in soil moisture is closely related to the changes in regional precipitation and temperature-based evapotranspiration^{8–10}. While the record-breaking heat and severe lack of

precipitation are blamed for the parched land in 2021, the ongoing worsening droughts are accompanied by increased evapotranspiration due to high temperature and decreased precipitation^{5,11,12}. Attribution studies have found that the rapid warming trend in the past half century over Central Asia is mainly forced by anthropogenic activities¹³. The observed changes in Central Asian precipitation contain both forced responses and internal variations^{14–16}. However, soil moisture, as the crucial indicator of agricultural and ecological droughts, has received less attention in understanding the cause of its observed changes in Central Asia.

There is a growing concern regarding the detection and attribution of long-term changes in soil moisture at regional or global

¹State Key Laboratory of Numerical Modeling for Atmospheric Sciences and Geophysical Fluid Dynamics, Institute of Atmospheric Physics, Chinese Academy of Sciences, Beijing, China. ²University of the Chinese Academy of Sciences, Beijing, China. e-mail: zhoutj@lasg.iap.ac.cn

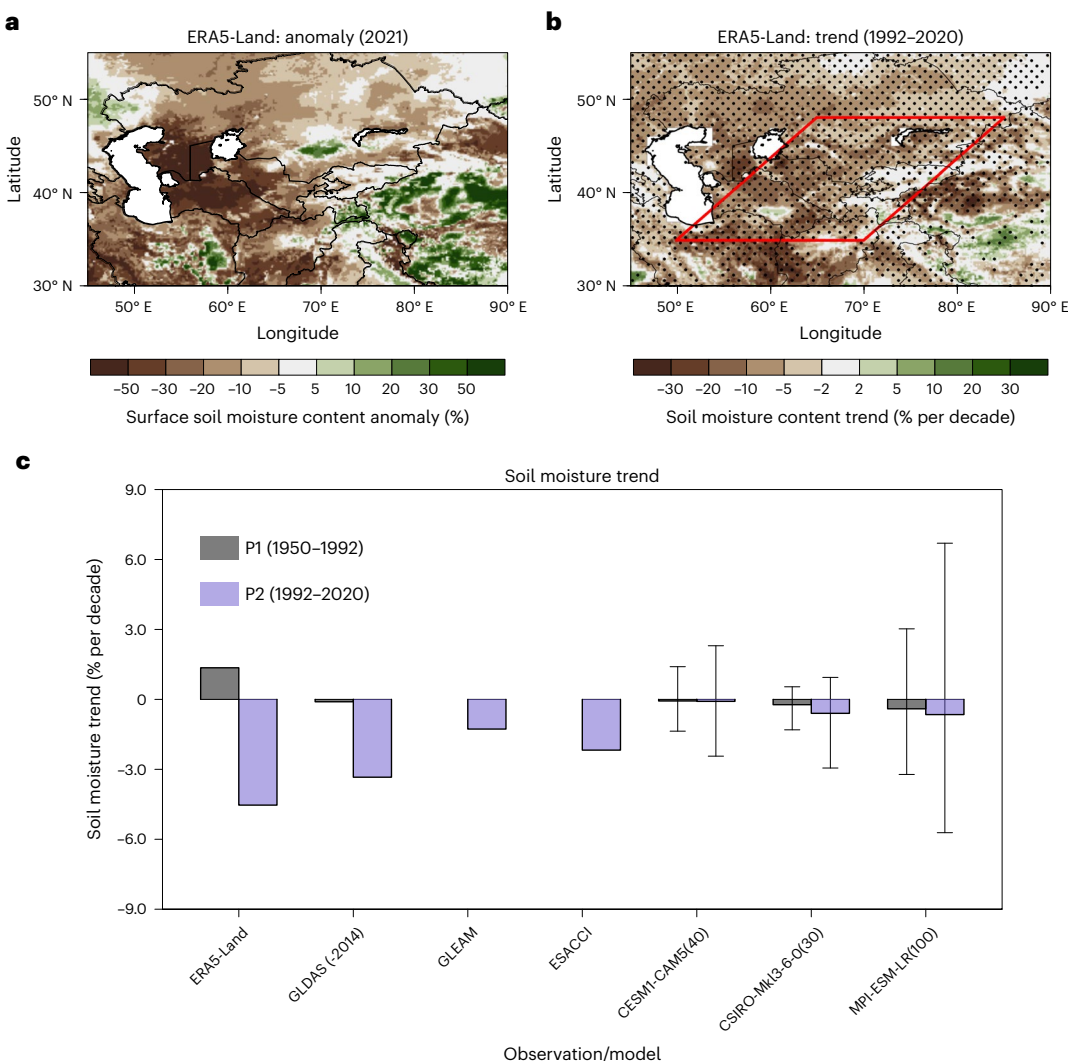


Fig. 1 | Drying trend over southern Central Asia. **a**, Surface soil moisture content anomaly (%) in AMJ 2021 relative to the climatological mean (1995–2014) derived from ERA5-Land. **b**, The trends of AMJ surface soil moisture content anomaly (% per decade) during 1992–2020 derived from ERA5-Land. Stippling indicates that the linear trends are significant at the 10% level according to the Mann–Kendall (MK) test. **c**, The trends in AMJ surface soil moisture content (% per decade) during 1950–1992 (grey) and 1992–2020 (blue) over southern Central

Asia (red box in **b**) obtained from ERA5-Land, GLDAS (ended 2014), GLEAM and ESACCI, and the ensemble mean of CESM1-CAM5, CSIRO-Mk3-6-0 and MPI-ESM-LR. The ensemble mean is calculated based on 40, 30 and 100 members for the three models, respectively. The error bars denote the range of the trends derived from all members for each model. As GLEAM and ESACCI are started in 1980 and 1978, respectively, the trends in P1 are not calculated.

scales. While soil moisture deficits are attributed to anthropogenic warming in America^{17,18}, Europe^{9,19,20}, the Northern Hemisphere²¹ and global land²², natural climate variability is also suggested to drive severe agricultural drought at regional scales^{8,18,23}. Understanding the influence of external forcing and internal variability on soil moisture change over Central Asia needs to separate the forced and unforced responses. The US Climate Variability and Predictability Program (CLIVAR) Working Group on Large Ensembles has set up a data archive containing large ensembles of historical and scenario simulations for several models²⁴. Unlike Coupled Model Intercomparison Project (CMIP)-like multi-model simulations with each model having few members, which are mainly used to reveal externally forced signals, large ensemble simulations from a single climate model are powerful tools to understand and quantify the relative contribution of internal variability and external forcing^{24–28}. In this study, based on three sets of large ensemble simulations, we provide evidence that the combined impact of external forcing and the phase change of the Interdecadal Pacific Oscillation (IPO), a long-term oscillation of sea

surface temperatures (SST) in the Pacific Ocean that can last from 20 to 30 years (refs. 29–31), has exacerbated agricultural droughts over water-scarce southern Central Asia in its early growing season since 1992. The IPO evolution could also modulate the externally forced drying trend in the near-term projection.

Observed drying trend

We focus on the surface soil moisture content in April–May–June (AMJ), which is the early time of the growing season in Central Asia³². Plants in this region mainly depend on shallow soil water and shallow ground-water to survive⁵. Since the 1950s, a decline in surface soil moisture has been seen over southern Central Asia (Extended Data Fig. 1). The drying tendency has accelerated since the 1990s with decreasing rates at -4.53% , -1.29% and -2.12% per decade during 1992–2020 for ERA5-Land, GLEAM and ESACCI, respectively (Fig. 1 and Extended Data Table 1). The soil moisture deficit in 2021 was one of the most severe droughts in the past 70 years, which was -11.79% lower than the climatological mean (1995–2014) based on ERA5-Land (Fig. 1a).

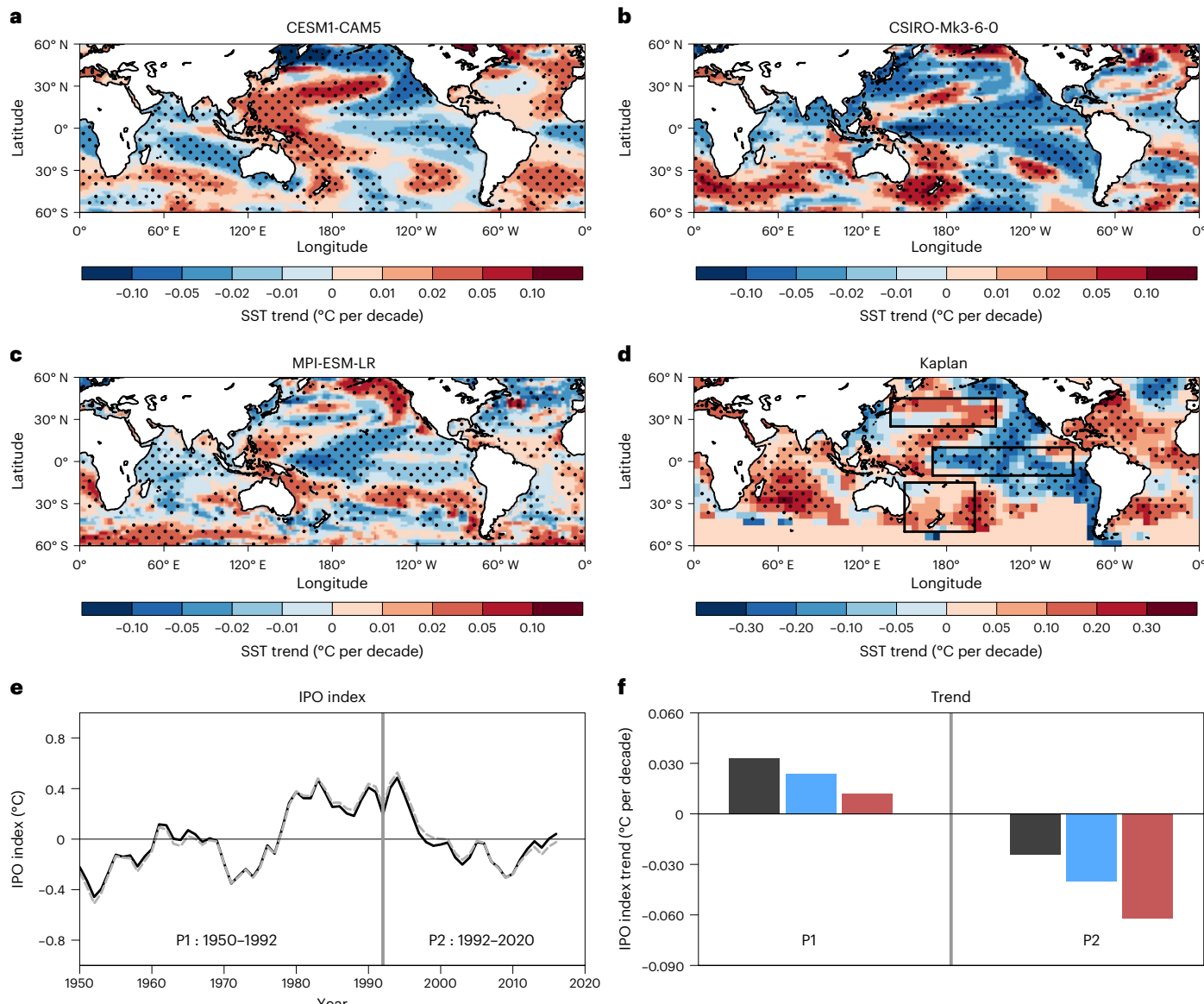


Fig. 2 | Impact of IPO on the AMJ soil moisture over southern Central Asia. **a–d**, Spatial distribution of trends in SST (°C per decade) for the difference between Min10 and ensemble mean of CESM1-CAM5 (a), CSIRO-Mk3-6-0 (b), MPI-ESM-LR (c) and the trends in SST derived from Kaplan (d) during 1992–2020. Stippling indicates that the linear trends are significant at the 10% level according to the

MK test. **e**, Time series of the 9-year running mean IPO index (°C) derived from Kaplan SST (black) and ERSST (grey). The vertical line denotes the year of 1992. **f**, The trends of IPO indices (°C per decade) derived from the ensemble mean of Max10 (Min10) during the period of 1950–1992 (1992–2020) derived from CESM1-CAM5 (black), CSIRO-Mk3-6-0 (blue) and MPI-ESM-LR (red).

Agricultural drought is related to meteorological factor changes, including temperature and precipitation³³. The surface soil moisture over southern Central Asia was negatively correlated with contemporaneous surface air temperature ($r = -0.62$; $p < 0.01$) (Extended Data Fig. 1a,b). The rising temperature increases the rate of evapotranspiration and depletes surface soil moisture^{34,35}. Central Asia has witnessed a significant warming trend in the past half century (Extended Data Fig. 2e,f). The observed warming trend was stronger after 1992, as indicated by the warming rate of 0.36 K per decade and 0.49 K per decade in 1950–1992 and 1992–2020, respectively. The enhanced warming rate after 1992 partly explained the amplified drying trend in soil moisture. Agricultural drought is also related to deficient rainfall. The surface soil moisture content was highly correlated with early precipitation in March–April–May ($r = 0.73$; $p < 0.01$) (Extended Data Fig. 1c,d). The deficiency of precipitation over an extended period of time can result in a water shortage for soil and environment, and a lag usually occurs

between the meteorological drought and agricultural drought^{36–38}. The decreased precipitation in spring and increased temperature-based evapotranspiration in AMJ result in imbalanced water supplies over southern Central Asia after 1992, which further leads to the significant drying trend (Fig. 1b and Extended Data Fig. 2).

Impact of external forcing

Is the accelerated drying trend since 1992 related to anthropogenic external forcing? The trends in surface soil moisture derived from the three sets of large ensemble simulations were examined (Fig. 1c). Under the same external forcing, 40 ensemble members of CESM1-CAM5 exhibited diverse soil moisture trends ranging from -1.36% to 1.40% per decade in 1950–1992 and -2.44% to 2.30% per decade in 1992–2020. There was a weak but significant drying trend of -0.07% per decade ($p < 0.05$) before 1992 and a larger drying trend of -0.08% per decade after 1992 for the ensemble mean (Fig. 1c and Extended Data

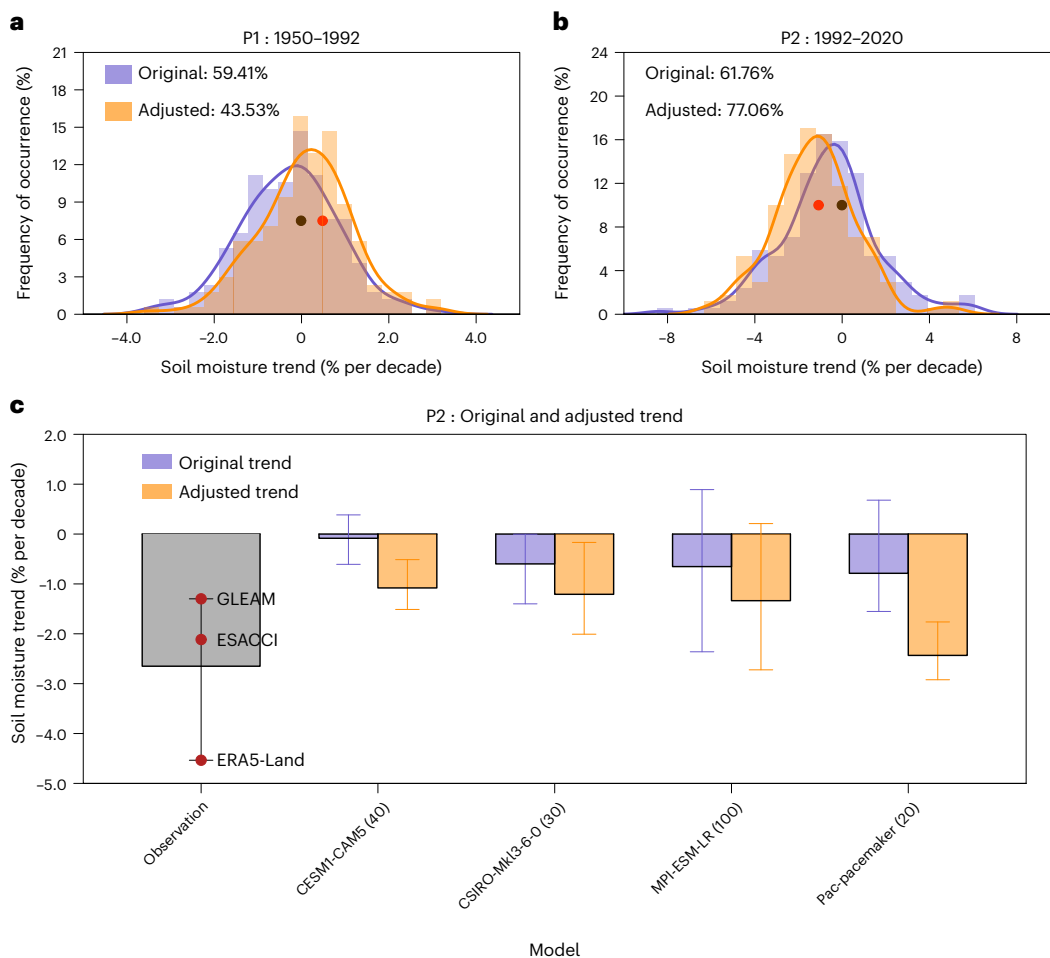


Fig. 3 | Adjustments of AMJ surface soil moisture content over southern Central Asia according to the observational IPO phase transition.

a, b, Histograms (bars) and fitted distribution (line) of the frequency of occurrence of the soil moisture content trends relative to 1995–2014 (% per decade) for the 170 members of the three models during 1950–1992 (**a**) and 1992–2020 (**b**) derived from the original results (orange) and those adjusted accounting for the influence of the observational IPO phase transition (blue). The black and red dots denote the trends for the ensemble mean without and with adjustments. The numbers denote the percentages for members with

negative trends. **c**, The original (blue) and adjusted trends (orange) in soil moisture content during 1992–2020 were obtained from CESM1-CAM5, CSIRO-Mk3-6-0 and MPI-ESM-LR, respectively. ‘Pac-pacemaker’ denotes the trends of the ensemble mean for the historical simulations (blue) and IPO pacemaker simulations (orange) of CESM1.1 during 1992–2013. The numbers after each of the climate models are ensembles analysed. The error bars denote the 25–75% range of all members. The grey bar denotes the average of ERA5-Land, GLEAM and ESACCI, and the error bar denotes the range of the three soil moisture products.

Table 1). The significant weak decreasing trends can also be found for CSIRO-Mk3-6-0 and MPI-ESM-LR in both periods, which were -0.23% and -0.60% per decade ($p < 0.01$) for CSIRO-Mk3-6-0 and -0.40% and -0.65% per decade ($p < 0.01$) for MPI-ESM-LR in 1950–1992 and 1992–2020, respectively (Fig. 1c). Hence the ensemble means of the large ensembles indicate that the external forcing has a weak but statistically significant contribution to the drying surface soil moisture over southern Central Asia since 1950, in particular after 1992.

Anthropogenic activities, especially the emission of greenhouse gases, has resulted in the significant warming trend in the past half century and the accelerated warming rate after 1990s¹³. The human-induced warming further leads to the increased evapotranspiration and decreased soil moisture. In addition, the spatial pattern of the long-term warming trend due to external forcing has suppressed spring precipitation over southern Central Asia^{15,39}, which was also favourable for the reduction in soil moisture content in AMJ.

Impact of the internal mode of IPO

While the ensemble mean simulation, as a measure of the response to external forcing, can reproduce the accelerated drying trend over

southern Central Asia after 1992, the simulated drying trend was far weaker than the observation (Fig. 1c and Extended Data Table 1). Among the large ensemble members, there were some realizations that can reproduce the observed magnitude change, indicating the contribution of internal variability (Fig. 1c). The SST trend difference between the Min10 (the mean of 10 members with the largest negative trends of soil moisture in 1992–2020) and the ensemble mean of all members were analysed and a negative phase of an IPO-like pattern was found, which featured a cooling trend over the tropical central eastern Pacific and a warming trend over the subtropical western Pacific (Fig. 2a–c). The IPO index decreased during 1992–2020 for the Min10 of all models (Fig. 2f). Following the accelerated drying trend over southern Central Asia since 1992, the positive-to-negative phase transition of the IPO was indeed seen in the observations (Fig. 2d,e).

Without the impact of external forcing, the positive-to-negative phase transition of IPO alone can lead to a decrease in soil moisture over southern Central Asia during 1992–2020. Following the transition of the IPO to a negative phase, anomalous SST trends will strengthen the Walker circulation and further enhance (suppress) convective activities over the Indo-western Pacific warm pool (central eastern

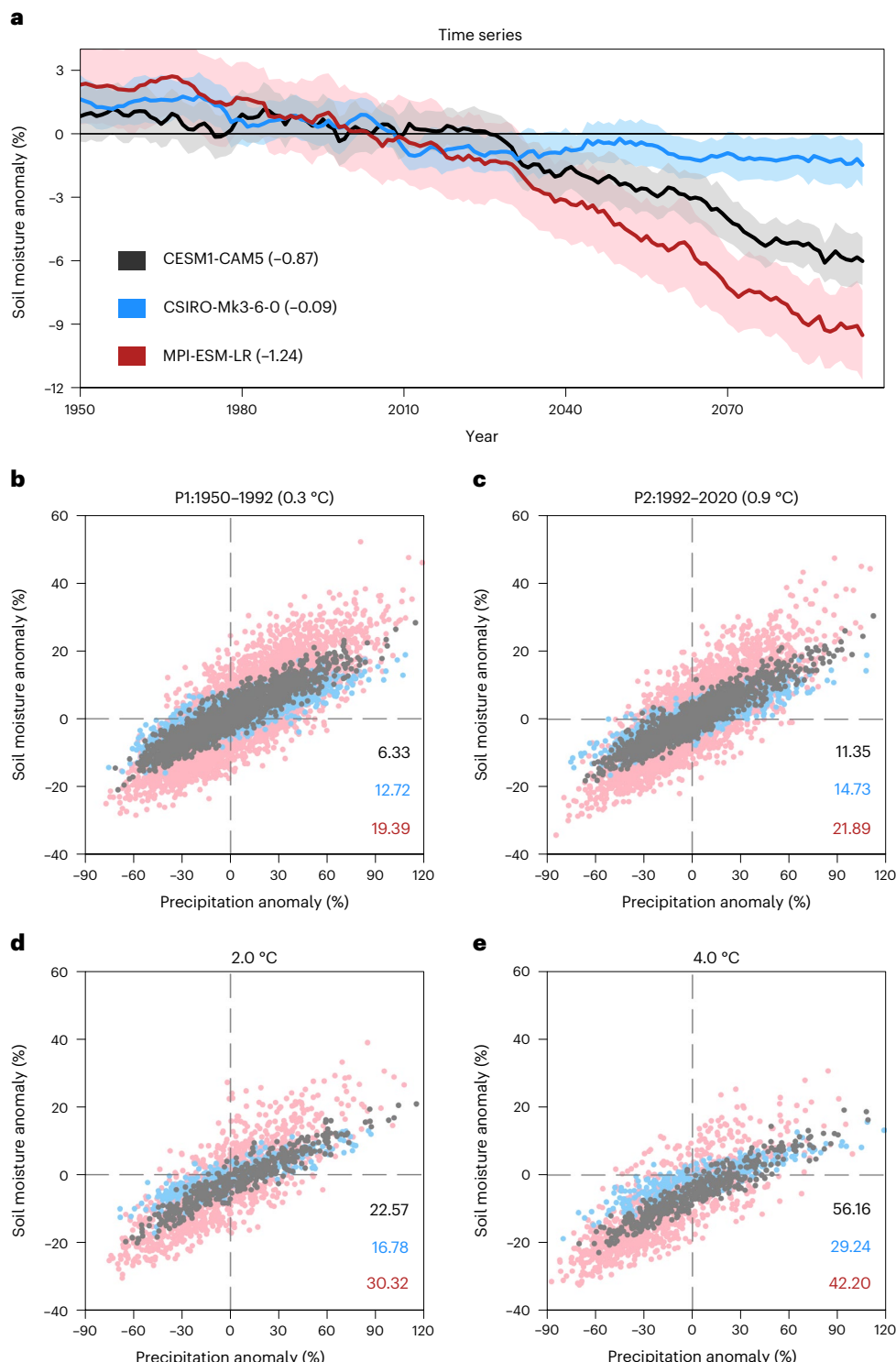


Fig. 4 | Future changes in AMJ surface soil moisture over southern Central Asia. **a.** Time series of the 9-year running mean soil moisture content anomalies (%) derived from CESM1-CAM5 (black), CSIRO-Mk3-6-0 (blue) and MPI-ESM-LR (red). The lines denote the results of the ensemble mean and the number denote the corresponding linear trends (% per decade) in 2021–2099; the light shades are for one standard deviation about the ensemble mean. **b–e.** The relationship

between the area-averaged AMJ surface soil moisture content anomaly (%) and spring (MAM) precipitation anomaly (%) during 1950–1992 (b) and 1992–2020 (c) and under 2 °C (d) and 4 °C (e) levels of global warming derived from CESM1-CAM5 (black), CSIRO-Mk3-6-0 (blue) and MPI-ESM-LR (red). The numbers denote the percentage of springs with negative soil moisture anomaly among springs with positive precipitation anomaly.

Pacific)⁴⁰. The increased latent heating associated with the enhanced precipitation in the Indo-western Pacific warm pool would stimulate westward-propagating baroclinic Rossby wave trains emanating from the western Pacific, which can lead to reduced rainfall over southern

Central Asia^{15,39,41,42}. In addition, the suppressed convective heating over the central eastern Pacific would stimulate poleward-propagating equivalent barotropic Rossby wave trains, which could extend eastward over North America and the North Atlantic into Eurasia, modulating

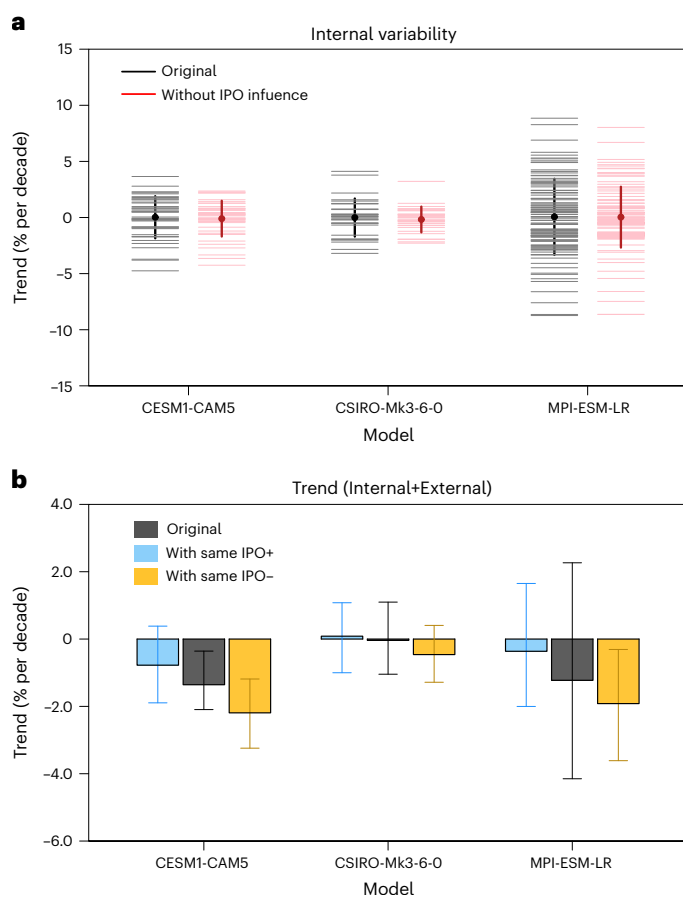


Fig. 5 | The changes in AMJ surface soil moisture content over southern Central Asia during 2021–2040 with and without IPO's influence. **a**, The linear trends of the internal component of the soil moisture content (% per decade) relative to 1995–2014 derived from 40, 30 and 100 members of CESM1-CAM5, CSIRO-Mk3-6-0 and MPI-ESM-LR, respectively. The grey thin lines denote the original results, and the red thin lines denote the trends with the IPO's influence being removed. The dots (thick lines) denote the corresponding ensemble mean (standard deviation, \pm SD). **b**, The original and adjusted trends in soil moisture content were obtained from CESM1-CAM5, CSIRO-Mk3-6-0 and MPI-ESM-LR, respectively. The bars denote the ensemble mean of the three models, and the error bars denote the 25–75% range of all members. The grey bars denote the original results, and the blue and yellow bars denote the trends with the same amplitude of a positive (+2SD per 2 decades) or a negative IPO ($-2SD$ per 2 decades) phase transition, respectively.

the precipitation over southern Central Asia^{14,42–45}. The precipitation changes further decreased the surface soil moisture over Central Asia. In addition, the IPO shifted from a negative to a positive phase during 1950–1992 in observations (Fig. 2e), which was favourable for more precipitation and wetter soil moisture over southern Central Asia before 1992 (Fig. 2f and Extended Data Fig. 3).

Attribution of observed drying trends to climate drivers

To quantify the relative contribution of external forcing and IPO, the IPO evolution was adjusted in each member based on the observed IPO index during the whole period (Methods). The original IPO-related soil moisture changes for each member were replaced by those induced by the observed IPO evolution. Therefore, the ensemble mean of the adjusted members represents the combination of the responses to external forcing and the observed IPO phase transition.

While the externally forced soil moisture trends during 1950–1992 ranged from -0.40% to -0.07% per decade for the three models, the negative-to-positive phase transition of IPO was favourable for wetter conditions over southern Central Asia at a rate of 0.22% to 0.55% per decade (Fig. 3a,c, Extended Data Fig. 4 and Extended Data Table 1). After adjustment, the IPO-induced increase in soil moisture offset the externally forced response, showing a weak trend in this period (-0.05% to 0.48% per decade). During 1992–2020, the adjustment with the observed positive-to-negative IPO transition decreased the soil moisture trend from -0.65% to -0.08% per decade to -1.34% to -1.08% per decade, which was closer to the observed trend (Fig. 3b,c, Extended Data Fig. 4 and Extended Data Table 1). The simulated IPO-induced trend was -1.00% to -0.61% per decade during 1992–2020, which was comparable to the externally forced drying trend. All the models converged towards a high probability of an accelerated drying trend over southern Central Asia after adjustment (Fig. 3b,c).

We further examined the contributions of IPO and anthropogenic external forcing by analysing the 20-member *IPO pacemaker simulations* of CESM1.1 and its corresponding historical simulations. In *IPO pacemaker simulations*, while the atmosphere and ocean are freely coupled in the historical simulations, the SST anomalies over the tropical Pacific vary synchronously with the observations (Methods). Whereas the historical simulations represent the response to external forcing, the pacemaker simulations represent the combined impact of observed IPO evolution and external forcing. The soil moisture decreased at rates of -0.79% per decade and -2.44% per decade for the ensemble mean of historical and pacemaker simulations, respectively. By considering both anthropogenic external forcing and IPO-related internal SST changes, the pacemaker simulations reasonably reproduced the observed drying trend after 1992 (Fig. 3c), further demonstrating the crucial contribution of internal variability of IPO.

Future changes

Under the representative concentration pathway version 8.5 (RCP8.5) emission scenario, the externally forced surface soil moisture content over southern Central Asia features a continued decreasing trend at rates of -0.87% , -0.09% and -1.24% per decade to the end of the century for the ensemble mean of CESM1-CAM5, CSIRO-Mk3-6-0 and MPI-ESM-LR, respectively (Fig. 4a). Multi-model projections of CMIP6 models also show a reduction in surface soil moisture over southern Central Asia under external forcing in both low- and high-emissions scenarios¹⁰. While the aggravated agricultural drought in AMJ will continue, the spring precipitation is projected to increase under the external forcing⁴⁶. To reveal the discrepancy among the future changes in precipitation and soil moisture content, we binned spring precipitation and AMJ surface air temperature over southern Central Asia into 5×5 or 10×10 bins and assessed the anomalies of surface soil moisture in each bin in observation and large ensemble simulations (Extended Data Fig. 5). For precipitation with similar magnitudes, surface soil moisture decreases as surface air temperature rises with promoted evapotranspiration. Among springs with positive precipitation anomalies, only 6.33% to 19.39% and 11.35% to 21.89% springs experienced negative soil moisture anomalies during 1950–1992 and 1992–2020, and the ratio would come to 16.78% to 30.32% and 29.24% to 56.16% for the $2\text{ }^{\circ}\text{C}$ and $4\text{ }^{\circ}\text{C}$ warming levels (Fig. 4c,d). Hence, although the precipitation will increase during the twenty-first century associated with the moistening atmosphere under external forcing, agricultural drought still will become more severe due to human-induced continuous warming and related increase of evapotranspiration.

The near-term externally forced projection can be amplified or reduced by internal variability^{40,47}. Given the evidence that the recent externally forced drying trend in southern Central Asia is accelerated due to the IPO evolution, will the IPO modulate the externally forced drying trend in the near term? We excluded all of the IPO's influence by removing the soil moisture variations that are linearly related to the

IPO index in each member (Methods). After the removal, the standard deviations (SDs) of the internal component of the linear trends during 2021–2040 among all members are reduced by 15% to 32% (Fig. 5a), indicating that the spread among different members can be partly explained by the IPO phase transition.

To reveal the role of the IPO on the near-term projection, we calculated the SD (0.23 °C) of the observational IPO index during 1950–2020 and assumed that the IPO will shift from +1SD to -1SD or from -1SD to +1SD in 2021–2040. The IPO phase change of 2SDs over a 20-year period (± 0.23 °C per decade) is comparable to the observational trends in 1950–1992 (0.15 °C per decade) and 1992–2020 (-0.28 °C per decade). We then replaced the original IPO-related soil moisture changes for each member by those induced by the assumed fixed IPO evolution (Methods). If an amplitude of -2SD of the IPO trend was predicted to be superimposed onto the external forcing from 2021 to 2040, the multi-model average would show a significant decrease in soil moisture by -1.52 (-2.19 to -0.46 for the model spread) % per decade (Fig. 5b), which is 0.65 (0.42, 0.83) % per decade drier than the externally forced drying trend (-0.87 (-1.36 , -0.04) % per decade), indicating nearly 75% enhancement of the drying trend. In contrast, if the IPO shifts from -1SD to +1SD, the negative-to-positive phase transition will weaken the externally forced drying trend by 0.52 (0.12, 0.86) % per decade, indicating nearly 60% weakening of the drying trend. The phase transition of the IPO could modulate the externally forced drying trend in the following decades and has a notable impact on the soil moisture trends over southern Central Asia in the near term.

Implications of a continued drying trend

The southern part of Central Asia has been facing an increase in aridity in its early growing season since the 1990s. The drying trend is not limited to surface soil but can also be found in deeper soil layers (Extended Data Fig. 6). Dominated by anthropogenic warming, agricultural droughts over southern Central Asia were expected to be exacerbated by the end of the century. The region with the highest population density at the foothill of the mountain was more likely to face a further enhanced agricultural drought (Extended Data Fig. 7). Superimposed onto the external forcing, the IPO evolution not only has intensified the decreasing tendency of soil moisture during 1992–2020 but would also modulate the externally forced drying trend in the near-term projection. Thus, improved IPO predictions are necessary for developing effective adaptation and mitigation strategies for decisionmakers of Central Asian countries. If the IPO turns into its warm phase in the next few decades, as some previous studies supposed⁴⁰, an amplitude of +2SD of the IPO trend will weaken the externally forced decreasing rate of surface soil moisture content by nearly 60% during 2021–2040.

In Central Asia, crop and livestock production is the dominant contributor to GDP and employment share^{33,48}. The increasingly serious agricultural droughts not only directly influence crops and livestock but are also a challenge for production, living, ecological environments, social stability and even regional security^{49,50}. A catastrophic drought during 2000–2001 revealed that due to structural factors, including rural poverty and unsustainable management of natural resources, agricultural drought in Central Asia was extremely likely to further lead to socioeconomic drought³³. Our results show that the decreasing trend in surface soil moisture since the 1990s will continue in the twenty-first century under the RCP8.5 scenario regardless of how the IPO changes unless we take ambitious climate action and reach global peaking of greenhouse gas emissions as soon as possible to achieve a climate-neutral world. In addition to agricultural drought, there are increasing risks of meteorological drought⁵¹ and hydrological drought^{52,53} in southern Central Asia. Overall, our findings have highlighted an urgent need of developing a thorough risk-management plan at sectoral, local, country and even multi-country levels to adapt and mitigate the enhanced agricultural droughts for food security and livestock production.

Online content

Any methods, additional references, Nature Portfolio reporting summaries, source data, extended data, supplementary information, acknowledgements, peer review information; details of author contributions and competing interests; and statements of data and code availability are available at <https://doi.org/10.1038/s41561-022-01111-0>.

References

1. Dai, A. & Zhao, T. Uncertainties in historical changes and future projections of drought. Part I: estimates of historical drought changes. *Climatic Change* **144**, 519–533 (2017).
2. Greve, P. et al. Global assessment of trends in wetting and drying over land. *Nat. Geosci.* **7**, 716–721 (2014).
3. Jiang, J. et al. Tracking moisture sources of precipitation over central Asia: a study based on the water-source-tagging method. *J. Clim.* **33**, 10339–10355 (2020).
4. Seneviratne, S. I. et al. in *Climate Change 2021: The Physical Science Basis* (eds Masson-Delmotte, V. et al.) (Cambridge Univ. Press, 2021).
5. Li, Z., Chen, Y., Fang, G. & Li, Y. Multivariate assessment and attribution of droughts in Central Asia. *Sci. Rep.* **7**, 1316 (2017).
6. Li, Z., Chen, Y., Li, W., Deng, H. & Fang, G. Potential impacts of climate change on vegetation dynamics in Central Asia. *J. Geophys. Res. Atmos.* **120**, 12345–12356 (2015).
7. Deng, H. & Chen, Y. Influences of recent climate change and human activities on water storage variations in Central Asia. *J. Hydrol.* **544**, 46–57 (2017).
8. Seager, R., Nakamura, J. & Ting, M. Mechanisms of seasonal soil moisture drought onset and termination in the southern Great Plains. *J. Hydrometeorol.* **20**, 751–771 (2019).
9. Teuling, A. J. et al. Evapotranspiration amplifies European summer drought. *Geophys. Res. Lett.* **40**, 2071–2075 (2013).
10. Douville, H. et al. in *Climate Change 2021: The Physical Science Basis* (eds. Masson-Delmotte, V. et al.) (Cambridge Univ. Press, 2021).
11. Dai, A. Increasing drought under global warming in observations and models. *Nat. Clim. Change* **3**, 52–58 (2013).
12. Barlow, M. & Hoell, A. Drought in the Middle East and Central-Southwest Asia during winter 2013/14. *Bull. Am. Meteorol. Soc.* **96**, S71–S76 (2015).
13. Peng, D., Zhou, T., Zhang, L. & Zou, L. Detecting human influence on the temperature changes in Central Asia. *Clim. Dyn.* **53**, 4553–4568 (2019).
14. Barlow, M. et al. A review of drought in the Middle East and Southwest Asia. *J. Clim.* **29**, 8547–8574 (2016).
15. Hoell, A., Funk, C. & Barlow, M. The forcing of Southwestern Asia teleconnections by low-frequency sea surface temperature variability during boreal winter. *J. Clim.* **28**, 1511–1526 (2015).
16. Jiang, J. & Zhou, T. Human-induced rainfall reduction in drought-prone northern central Asia. *Geophys. Res. Lett.* **48**, e2020GL092156 (2021).
17. Williams, A. P. et al. Contribution of anthropogenic warming to California drought during 2012–2014. *Geophys. Res. Lett.* **42**, 6819–6828 (2015).
18. Williams, A. P. et al. Large contribution from anthropogenic warming to an emerging North American megadrought. *Science* **368**, 314–318 (2020).
19. Samaniego, L. et al. Anthropogenic warming exacerbates European soil moisture droughts. *Nat. Clim. Change* **8**, 421–426 (2018).
20. García-Herrera, R. et al. The European 2016/17 drought. *J. Clim.* **32**, 3169–3187 (2019).
21. Mueller, B. & Zhang, X. Causes of drying trends in northern hemispheric land areas in reconstructed soil moisture data. *Clim. Change* **134**, 255–267 (2016).

22. Gu, X. et al. Attribution of global soil moisture drying to human activities: a quantitative viewpoint. *Geophys. Res. Lett.* **46**, 2573–2582 (2019).

23. Coats, S. et al. Internal ocean–atmosphere variability drives megadroughts in western North America. *Geophys. Res. Lett.* **43**, 9886–9894 (2016).

24. Deser, C. et al. Insights from Earth system model initial-condition large ensembles and future prospects. *Nat. Clim. Change* **10**, 277–286 (2020).

25. Hawkins, E. & Sutton, R. The potential to narrow uncertainty in regional climate predictions. *Bull. Am. Meteorol. Soc.* **90**, 1095–1108 (2009).

26. Deser, C., Knutti, R., Solomon, S. & Phillips, A. S. Communication of the role of natural variability in future North American climate. *Nat. Clim. Change* **2**, 775–779 (2012).

27. Murphy, J. M. et al. Transient climate changes in a perturbed parameter ensemble of emissions-driven Earth system model simulations. *Clim. Dyn.* **43**, 2855–2885 (2014).

28. Huang, X. et al. The recent decline and recovery of Indian summer monsoon rainfall: relative roles of external forcing and internal variability. *J. Clim.* **33**, 5035–5060 (2020).

29. Zhang, Y., Wallace, J. M. & Battisti, D. S. ENSO-like interdecadal variability: 1900–93. *J. Clim.* **10**, 1004–1020 (1997).

30. Power, S., Casey, T., Folland, C., Colman, A. & Mehta, V. Inter-decadal modulation of the impact of ENSO on Australia. *Clim. Dyn.* **15**, 319–324 (1999).

31. Henley, B. J. et al. A tripole index for the Interdecadal Pacific Oscillation. *Clim. Dyn.* **45**, 3077–3090 (2015).

32. Wu, L., Ma, X., Dou, X., Zhu, J. & Zhao, C. Impacts of climate change on vegetation phenology and net primary productivity in arid Central Asia. *Sci. Total Environ.* **796**, 149055 (2021).

33. FAO. *Drought Characteristics and Management in Central Asia and Turkey* (FAO Water Reports, 2017).

34. Cai, W., Cowan, T., Briggs, P. & Raupach, M. Rising temperature depletes soil moisture and exacerbates severe drought conditions across southeast Australia. *Geophys. Res. Lett.* **36**, L21709 (2009).

35. Kidron, G. J. & Kronenfeld, R. Temperature rise severely affects pan and soil evaporation in the Negev Desert. *Ecohydrology* **9**, 1130–1138 (2016).

36. Xu, Y., Zhang, X., Hao, Z., Singh, V. P. & Hao, F. Characterization of agricultural drought propagation over China based on bivariate probabilistic quantification. *J. Hydrol.* **598**, 126194 (2021).

37. Bae, H. et al. Characteristics of drought propagation in South Korea: relationship between meteorological, agricultural, and hydrological droughts. *Nat. Hazards* **99**, 1–16 (2019).

38. Wang, W., Ertsen, M. W., Svoboda, M. D. & Hafeez, M. Propagation of drought: from meteorological drought to agricultural and hydrological drought. *Adv. Meteorol.* **2016**, 127897 (2016).

39. Hoell, A., Funk, C., Barlow, M. & Cannon, F. in *Climate Extremes: Patterns and Mechanisms* (eds Wang, S. et al.) 283–298 (American Geophysical Union, 2017).

40. Wu, M. et al. A very likely weakening of Pacific Walker Circulation in constrained near-future projections. *Nat. Commun.* **12**, 6502 (2021).

41. Hoell, A., Barlow, M., Cannon, F. & Xu, T. Oceanic origins of historical southwest Asia precipitation during the boreal cold season. *J. Clim.* **30**, 2885–2903 (2017).

42. Jiang, J., Zhou, T., Chen, X. & Wu, B. Central Asian precipitation shaped by the tropical Pacific decadal variability and the Atlantic multidecadal variability. *J. Clim.* **34**, 7541–7553 (2021).

43. Barlow, M. A. & Tippett, M. K. Variability and predictability of Central Asia river flows: antecedent winter precipitation and large-scale teleconnections. *J. Hydrometeorol.* **9**, 1334–1349 (2008).

44. Hoell, A., Barlow, M. & Saini, R. Intraseasonal and seasonal-to-interannual Indian Ocean convection and hemispheric teleconnections. *J. Clim.* **26**, 8850–8867 (2013).

45. Rana, S., McGregor, J. & Renwick, J. Dominant modes of winter precipitation variability over Central Southwest Asia and inter-decadal change in the ENSO teleconnection. *Clim. Dyn.* <https://doi.org/10.1007/s00382-019-04889-9> (2019).

46. Jiang, J., Zhou, T., Chen, X. & Zhang, L. Future changes in precipitation over Central Asia based on CMIP6 projections. *Environ. Res. Lett.* **15**, 054009 (2020).

47. Huang, X. et al. South Asian summer monsoon projections constrained by the interdecadal Pacific oscillation. *Sci. Adv.* **6**, eaay6546 (2020).

48. Varis, O. Resources: curb vast water use in Central Asia. *Nature* **514**, 27–29 (2014).

49. Farah, P. in *ENERGY: POLICY, LEGAL AND SOCIAL-ECONOMIC ISSUES UNDER THE DIMENSIONS OF SUSTAINABILITY AND SECURITY* (eds Farah, P. & Rossi, P.) 179–193 (Imperial College Press & World Scientific Publishing, 2015).

50. Wang, X., Chen, Y., Li, Z., Fang, G. & Wang, Y. Development and utilization of water resources and assessment of water security in Central Asia. *Agric. Water Manag.* **240**, 106297 (2020).

51. Peng, D., Zhou, T., Zhang, L., Zhang, W. & Chen, X. Observationally constrained projection of the reduced intensification of extreme climate events in Central Asia from 0.5 °C less global warming. *Clim. Dyn.* **54**, 543–560 (2020).

52. Pokhrel, Y. et al. Global terrestrial water storage and drought severity under climate change. *Nat. Clim. Change* **11**, 226–233 (2021).

53. Zhao, T. & Dai, A. CMIP6 model-projected hydroclimatic and drought changes and their causes in the 21st century. *J. Clim.* <https://doi.org/10.1175/JCLI-D-21-0442.1> (2021).

Publisher's note Springer Nature remains neutral with regard to jurisdictional claims in published maps and institutional affiliations.

Open Access This article is licensed under a Creative Commons Attribution 4.0 International License, which permits use, sharing, adaptation, distribution and reproduction in any medium or format, as long as you give appropriate credit to the original author(s) and the source, provide a link to the Creative Commons license, and indicate if changes were made. The images or other third party material in this article are included in the article's Creative Commons license, unless indicated otherwise in a credit line to the material. If material is not included in the article's Creative Commons license and your intended use is not permitted by statutory regulation or exceeds the permitted use, you will need to obtain permission directly from the copyright holder. To view a copy of this license, visit <http://creativecommons.org/licenses/by/4.0/>.

© The Author(s) 2023

Methods

Soil moisture

In this study, we focused on agricultural drought by analysing the surface soil moisture content. Multi-source soil moisture products were used, including: (1) ERA5-Land reanalysis soil moisture data derived from the Land Surface Scheme of the operational Integrated Forecasting System used at European Centre for Medium-Range Weather Forecasts with a spatial resolution of $0.1 \times 0.1^\circ$ during 1950–2021, soil moisture contents over 0–7 cm, 7–28 cm, 28–100 cm and 100–289 cm are available⁵⁴; (2) the soil moisture product derived from the NASA's Global Land Data Assimilation System (GLDAS Noah) with a spatial resolution of $1 \times 1^\circ$ during 1948–2014, soil moisture contents over 0–10 cm, 10–40 cm, 40–100 cm and 100–200 cm are available⁵⁵; (3) the soil moisture product derived from the Global Land Evaporation Amsterdam Model (GLEAM v3.3a) with a spatial resolution of $0.25 \times 0.25^\circ$ during 1980–2021, soil moisture contents at surface layer (0–10 cm) and root zone are available⁵⁶; (4) the multi-sensor soil moisture dataset obtained from European Space Agency (ESA) in the implementation of the Global Basic Climate Change Initiative (CCI) with a spatial resolution of $0.25 \times 0.25^\circ$ during 1978–2021, which merged soil moisture observations derived from multiple active and passive satellite remote sensing instruments in the microwave domain and was adjusted based on break correction; only soil moisture content at the surface layer is available⁵⁷.

Climate data

The monthly precipitation provided by the Met Office Hadley Center gridded land surface extremes indices (HadEX3)⁵⁸ was used to examine the relationship between surface soil moisture and regional precipitation. Monthly gridded observational temperature from the Berkeley Earth Surface Temperature dataset (BEST)⁵⁹ was used to reveal the relationship between surface soil moisture and regional temperature. Details of the datasets are provided in Supplementary Table 1.

Large simulations

To investigate the impact of internal variability and external forcing, three sets of large ensemble simulations from the US CLIVAR Working Group on Large Ensembles were used, including CESM1-CAM5, CSIRO-Mk3-6-0 and MPI-ESM-LR. These simulations are selected because at least 30 members are available and monthly surface soil moisture content is provided. A detailed introduction of the models is provided in Supplementary Table 2. The historical simulations covering the period of 1850–2005 were driven by observed historical changes in radiative forcing following phase 5 of the Coupled Model Intercomparison Project (CMIP5)⁶⁰. To satisfy the analysis of long-term trends during 1950–2020, the simulations were extended to 2020 following the representative concentration pathway version 8.5 (RCP8.5) emissions scenario. The three models can reasonably reproduce the climatological mean of surface soil moisture (Supplementary Fig. 1), the long-term trends in surface temperature (Supplementary Fig. 2) and the relationship between precipitation over southern Central Asia and moisture transport from the Indian Ocean (Supplementary Fig. 3).

Pacemaker simulations

To confirm the impact of IPO on Central Asian soil moisture, the results of 20-member coupled model ensembles of tropical Pacific 'pacemaker' simulations performed with the National Center for Atmospheric Research Community Earth System Model version 1 (NCAR CESM1) were compared with the corresponding historical simulations. The Pacific pacemaker simulations were forced by historical radiative forcing through 2005 and the RCP8.5 radiative forcing thereafter like the historical simulations, but the SST anomaly was nudged to be observations in the eastern tropical Pacific. Further details on the model and simulations can be found in Deser et al.^{61,62}.

Separating externally forced and internally unforced signals

Take CESM1-CAM5 as an example. A certain variable $V(i)$ of member i in CESM1-CAM5 is influenced by both external forcing and internal variability. As all members are driven by the same external forcing, the ensemble means of $V(i)$ for all members can be regarded as the response to external forcing V_{forced} and are represented as:

$$V_{\text{forced}} = (V(i))_{\text{EM}}, i = 1, 2, \dots, n - 1, n \quad (1)$$

Thus, $V(i)$ can be separated as:

$$V(i) = V_{\text{forced}} + V_{\text{internal}}(i), i = 1, 2, \dots, n - 1, n, \quad (2)$$

where $V_{\text{internal}}(i)$ is the internal component estimated as the residual of the original $V(i)$ minus the model forced response V_{forced} .

IPO definition

The IPO index is defined as the difference between the SST anomalies averaged over the central equatorial Pacific (10°S – 10°N , 170°E – 90°W) and the average of the SST anomalies in the Northwest (25°N – 45°N , 140°E – 145°W) and Southwest Pacific (50°S – 15°S , 150°E – 160°W) following Henley et al.³¹. The definition of the IPO index varies among different studies with similar phase transitions^{30,31,63}. We calculated the IPO index based on area-averaged SST anomalies rather than the leading mode of SST in the Pacific Ocean for easier calculation and direct comparison between observations and model simulations. There is a high consistency between the IPO indices derived from the Kaplan SST dataset⁶⁴ and Extended Reconstructed Sea Surface Temperature (ERSST)⁶⁵ with a correlation coefficient of 0.99 ($p < 0.01$). In particular, the IPO index for each ensemble member of the simulations was obtained by the internal part of SST, namely $SST_{\text{internal}}(i)$.

Adjustment of soil moisture based on observational IPO

An 'adjustment' method following Salzmann and Cherian⁶⁶ was used in this study. The core idea of this method is replacing the original simulated IPO-related soil moisture trend with that induced by observed IPO evolution, which is expressed as:

$$\partial_t V_{\text{adj}}(i) = \partial_t V_{\text{forced}} + \partial_t V_{\text{internal,adj}}(i), i = 1, 2, \dots, n - 1, n, \quad (3)$$

where:

$$\partial_t V_{\text{internal,adj}}(i) = \partial_t V_{\text{internal}}(i) + A_{\text{internal}}(i). \quad (4)$$

$A_{\text{internal}}(i)$ is the adjusted term and can be expressed as:

$$A_{\text{internal}}(i) = -r_{V,\text{IPO}}(i)[\partial_t \text{IPO}(i) - \partial_t \text{IPO}_{\text{OBS}}], \quad (5)$$

where $r_{V,\text{IPO}}(i)$ is the regression coefficient of the soil moisture regressed onto the IPO index during the study period, reflecting the response rate of soil moisture to IPO evolution for member i . $r_{V,\text{IPO}}(i)\partial_t \text{IPO}(i)$ denotes the original IPO-related soil moisture trend in member i , and $r_{V,\text{IPO}}(i)\partial_t \text{IPO}_{\text{OBS}}$ denotes the soil moisture trend related to the observed IPO evolution with the same amplitude. While $\partial_t V_{\text{forced}}$ represents the response of soil moisture to external forcing, the ensemble mean of $\partial_t V_{\text{internal,adj}}(i)$ can represent the soil moisture trend contributed by the observed IPO evolution.

Removing IPO's influence

To remove the IPO's influence, we calculated the IPO index for each member and removed the soil moisture variations that are linearly related to the IPO index through a linear regression, which is expressed as:

$$V_{\text{non-IPO}}(i, t) = V(i, t) - r_{V,\text{IPO}}(i) \times \text{IPO}(i, t), i = 1, 2, \dots, n - 1, n. \quad (6)$$

Statistical analysis

The area-weighted method was used to calculate the regional average. A 9-year running mean was applied to observation and model outputs to isolate the interdecadal signal. The Theil–Sen trend estimation method was used in this study to estimate the linear trend, which is not sensitive to outliers⁶⁷. The non-parametric MK test was used to detect the presence of the trends^{68,69}.

Data availability

The large ensemble simulations are publicly available at the multi-model large ensemble archive of NCAR Climate Data Gateway (<https://www.cesm.ucar.edu/projects/community-projects/MMLEA/>). The pacemaker simulations of CESM1.1 are available at <https://www.earthsystemgrid.org/dataset/ucar.cgd.ccsm4.pac-pacemaker.html>. ERA5-Land soil products are available from <https://cds.climate.copernicus.eu/cdsapp#!/dataset/reanalysis-era5-land-monthly-means?tab=form>. GLDAS Noah driving surface soil moisture content is from <https://disc.gsfc.nasa.gov/datasets?keywords=GLDAS>. GLEAM soil moisture products are available from <https://www.gleam.eu/>. ESACCI soil moisture product can be downloaded from <https://esa-soilmoisture-cci.org/>. HadEX3 precipitation is publicly available at <https://www.met-office.gov.uk/hadobs/hadex3/index.html>. BEST is available at <http://berkeleyearth.org/data/>. Kaplan SST data and ERSST are provided by the National Oceanic and Atmospheric Administration (NOAA) Physical Sciences Laboratory (PSL) at <https://psl.noaa.gov/data/gridded/>.

Code availability

The data in this study is analysed with NCAR Command Language. All relevant codes used in this work are available upon request from the corresponding author.

References

54. Balsamo, G. et al. ERA-Interim/Land: a global land surface reanalysis data set. *Hydrol. Earth Syst. Sci.* **19**, 389–407 (2015).
55. Rodell, M. et al. The Global Land Data Assimilation System. *Bull. Am. Meteorol. Soc.* **85**, 381–394 (2004).
56. Martens, B. et al. GLEAM v3: satellite-based land evaporation and root-zone soil moisture. *Geosci. Model Dev.* **10**, 1903–1925 (2017).
57. Preimesberger, W., Scanlon, T., Su, C.-H., Gruber, A. & Dorigo, W. Homogenization of structural breaks in the global ESA CCI soil moisture multisatellite climate data record. *IEEE Trans. Geosci. Remote Sens.* **59**, 2845–2862 (2021).
58. Dunn, R. J. H. et al. Development of an updated global land in situ-based data set of temperature and precipitation extremes: HadEX3. *J. Geophys. Res. Atmos.* **125**, e2019JD032263 (2020).
59. Rohde, R., Muller, R., Jacobsen, R., Perlmutter, S. & Mosher, S. Berkeley Earth temperature averaging process. *Geoinf. Geostat.* **1**, 2 (2013).
60. Taylor, K. E., Stouffer, R. J. & Meehl, G. A. An overview of CMIP5 and the experiment design. *Bull. Am. Meteorol. Soc.* **93**, 485–498 (2012).
61. Deser, C., Simpson, I. R., McKinnon, K. A. & Phillips, A. S. The Northern Hemisphere extratropical atmospheric circulation response to ENSO: how well do we know it and how do we evaluate models accordingly? *J. Clim.* **30**, 5059–5082 (2017).
62. Deser, C., Guo, R. & Lehner, F. The relative contributions of tropical Pacific sea surface temperatures and atmospheric internal variability to the recent global warming hiatus. *Geophys. Res. Lett.* **44**, 7945–7954 (2017).
63. Henley, B. J. Pacific decadal climate variability: indices, patterns and tropical–extratropical interactions. *Glob. Planet. Change* **155**, 42–55 (2017).
64. Kaplan, A. et al. Analyses of global sea surface temperature 1856–1991. *J. Geophys. Res. Ocean.* **103**, 18567–18589 (1998).
65. Huang, B. et al. Extended reconstructed sea surface temperature, Version 5 (ERSSTv5): upgrades, validations, and intercomparisons. *J. Clim.* **30**, 8179–8205 (2017).
66. Salzmann, M. & Cherian, R. On the enhancement of the Indian summer monsoon drying by Pacific multidecadal variability during the latter half of the twentieth century. *J. Geophys. Res. Atmos.* **120**, 9103–9118 (2015).
67. Ohlson, J. A. & Kim, S. Linear valuation without OLS: the Theil–Sen estimation approach. *SSRN Electron. J.* <https://doi.org/10.2139/ssrn.2276927> (2013).
68. Mann, H. B. Nonparametric tests against trend. *Econometrica* **13**, 245–259 (1945).
69. Kendall, M. G. *Rank Correlation Methods* (Hafner Publishing Company, 1955).

Acknowledgements

This study is jointly supported by the National Natural Science Foundation of China (41988101, T.Z.), the Strategic Priority Research Program of the Chinese Academy of Sciences (XDA20060102, T.Z.) and China Postdoctoral Science Foundation (2022M713093, J.J.).

Author contributions

T.Z. designed the study, provided comments and revised the manuscript. J.J. conducted the analysis and drafted the manuscript.

Competing interests

The authors declare no competing interests.

Additional information

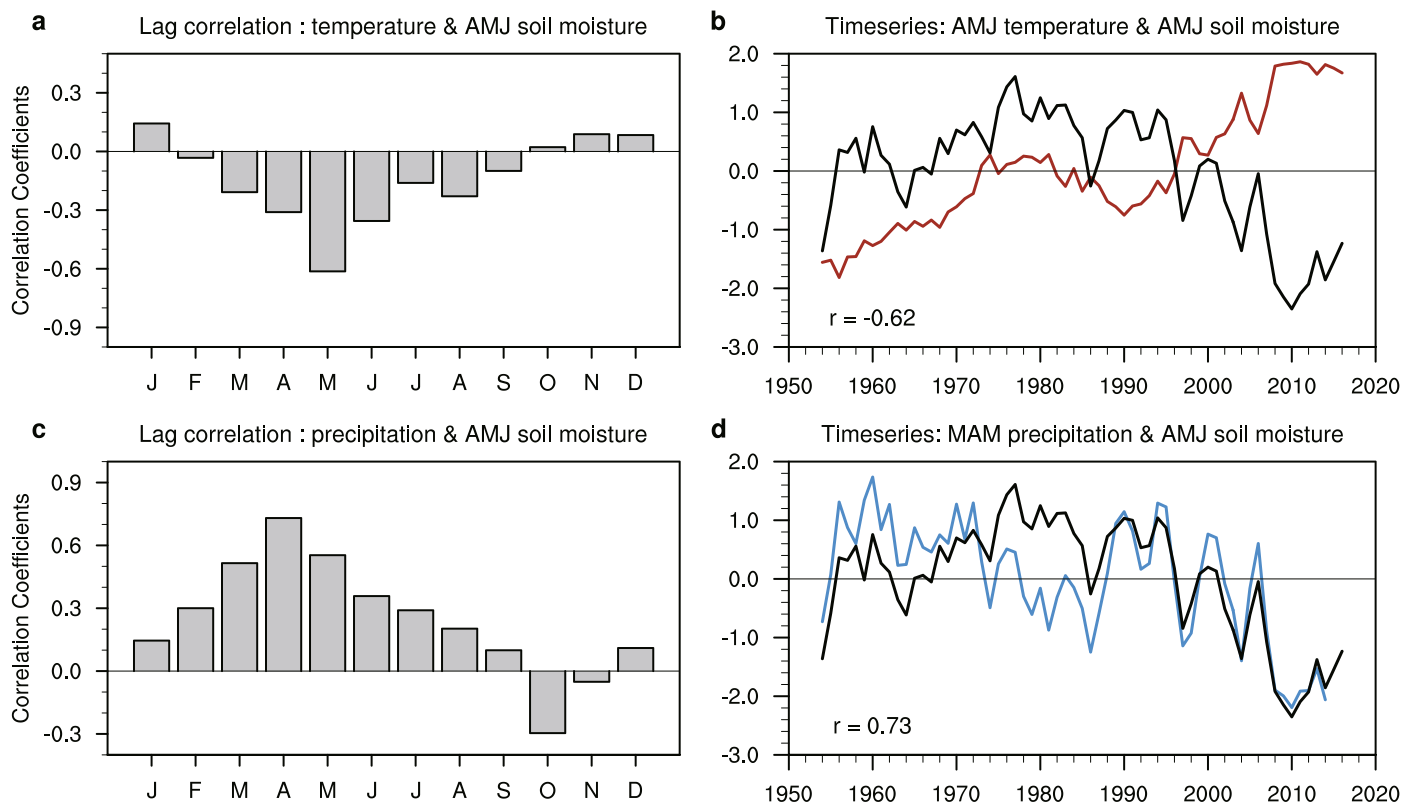
Extended data is available for this paper at <https://doi.org/10.1038/s41561-022-01111-0>.

Supplementary information The online version contains supplementary material available at <https://doi.org/10.1038/s41561-022-01111-0>.

Correspondence and requests for materials should be addressed to Tianjun Zhou.

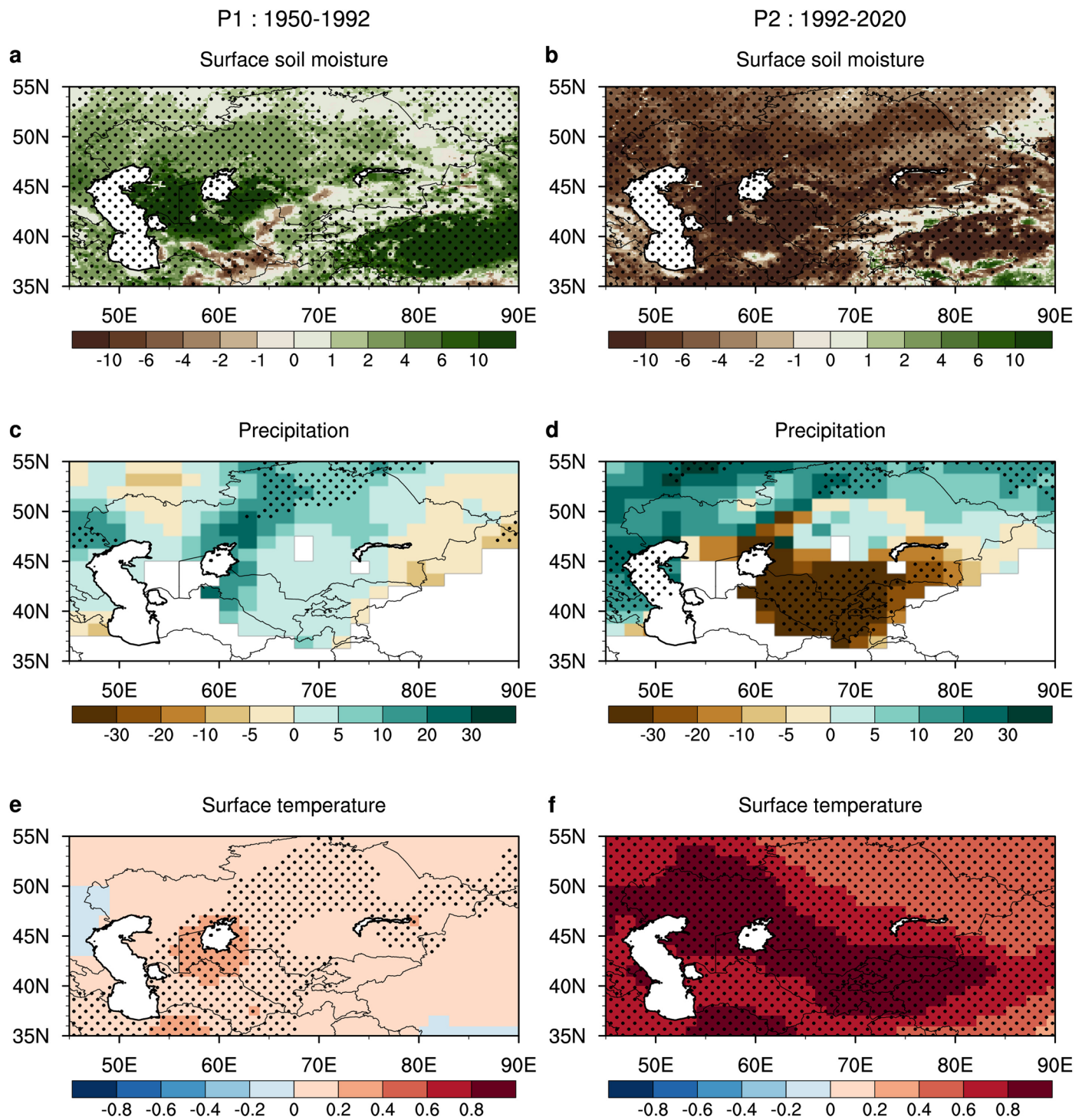
Peer review information *Nature Geoscience* thanks the anonymous reviewers for their contribution to the peer review of this work. Primary Handling Editors: Tamara Goldin, in collaboration with the *Nature Geoscience* team.

Reprints and permissions information is available at www.nature.com/reprints.



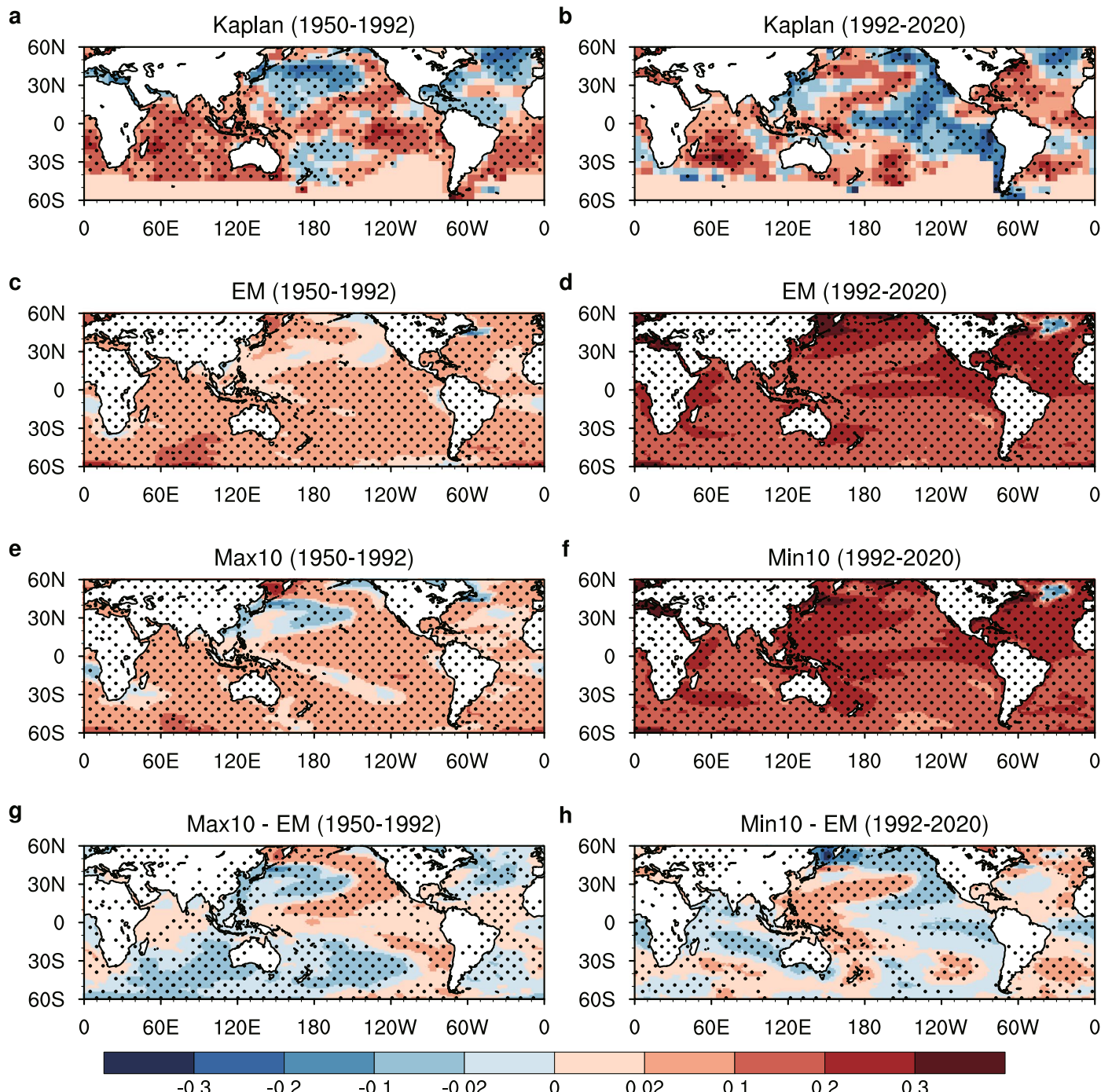
Extended Data Fig. 1 | Relationship between surface soil moisture and surface air temperature, precipitation. **a,c**, Lagged correlation coefficients between AMJ surface soil moisture content and surface air temperature (**a**) and precipitation (**c**) over southern Central Asia. **b,d**, Time series of normalized 9-year running average of AMJ surface soil moisture (black), AMJ surface

temperature (red, **b**) and MAM precipitation (blue, **d**) during 1950–2020. The numbers denote the corresponding correlation coefficients ($p < 0.01$). Data source: HadEX3 (precipitation), BEST (temperature) and ERA5-Land (surface soil moisture content).



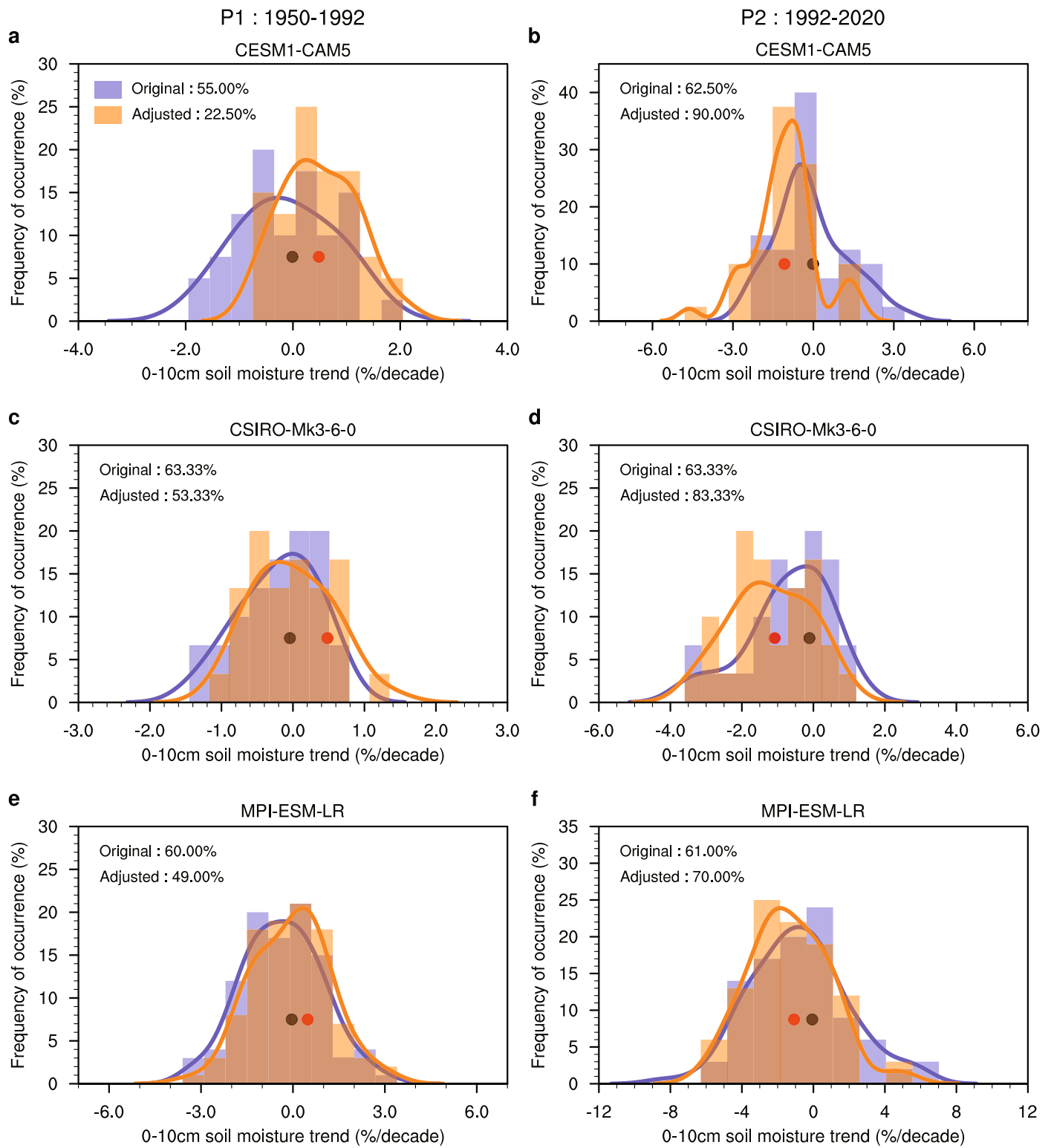
Extended Data Fig. 2 | The trend in AMJ surface soil moisture and related climatic variables over Central Asia. **a–f**, The trends in AMJ surface soil moisture content (**a, b**; %/decade), MAM precipitation (**c, d**; %/decade) and AMJ surface temperature (**e, f**; %/decade) over Central Asia during 1950–1992 (**a, c, e**)

and 1992–2020 (**b, d, f**). Stippling indicates that the linear trends are significant at the 10% level according to the MK test. Data source: HadEX3 (precipitation), BEST (temperature) and ERA5-Land (surface soil moisture content).

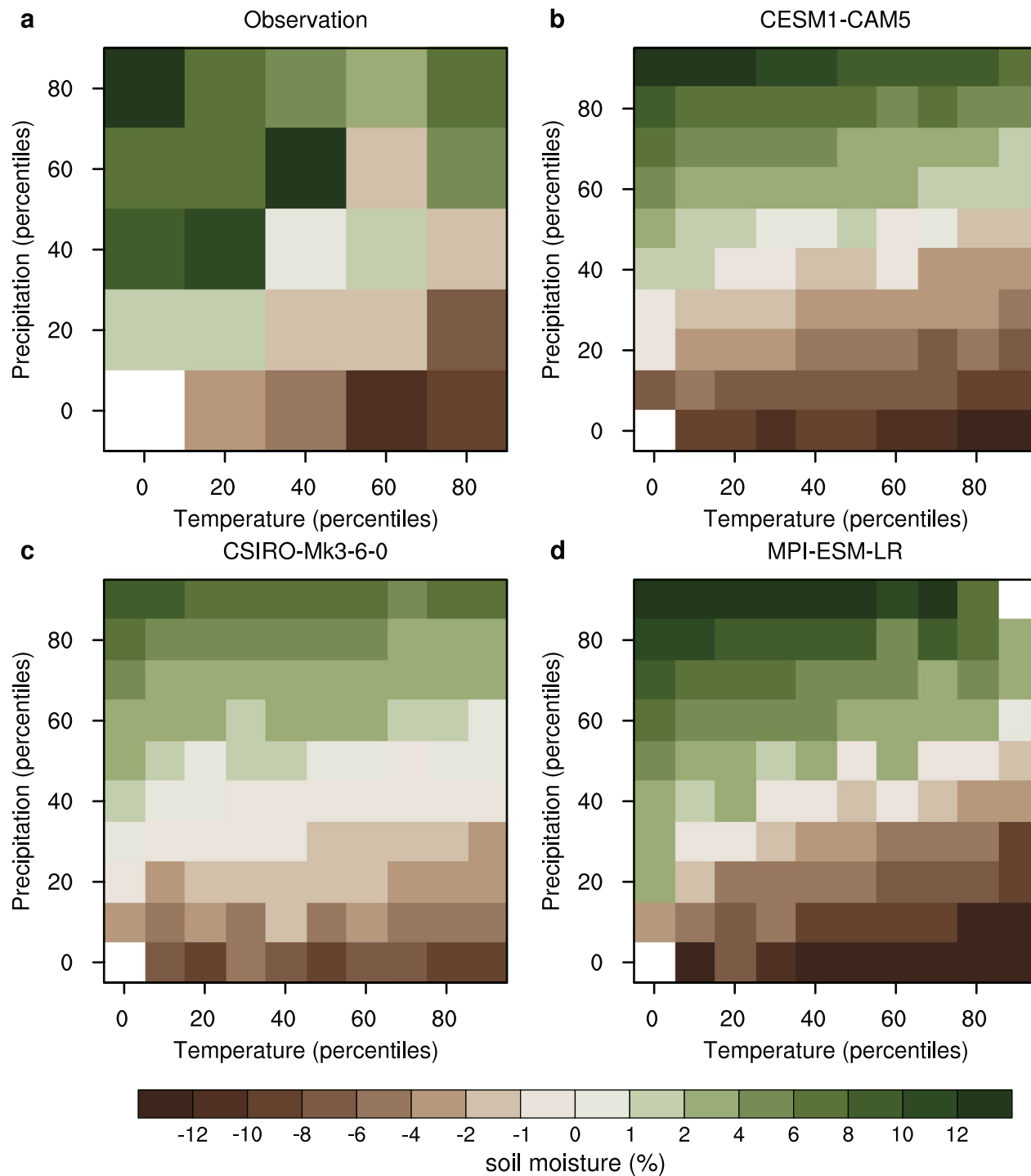


Extended Data Fig. 3 | Sea surface temperature anomalies associated with the internal variability of AMJ surface soil moisture content over southern Central Asia. a–h. Spatial distribution of trends in SST for Kaplan (a,b), ensemble mean (c,d), Max10 (e), Min10 (f), the difference between Max10 and ensemble

mean (g) and the difference between Min10 and ensemble mean (h) of CESM1-CAM5 during 1950–1992 (a,c,e,g) and 1992–2020 (b,d,f,h). Stippling indicates that the linear trends are significant at the 10% level according to the MK test.



Extended Data Fig. 4 | The trends in surface soil moisture content over southern Central Asia with and without adjustment. As in Fig. 3a,b, but are results for CESM1-CAM5 (a,b), CSIRO-Mk3-6.0 (c,d) and MPI-ESM-LR (e,f), respectively, in 1950–1992 (a,c,e) and 1992–2020 (b,d,f).

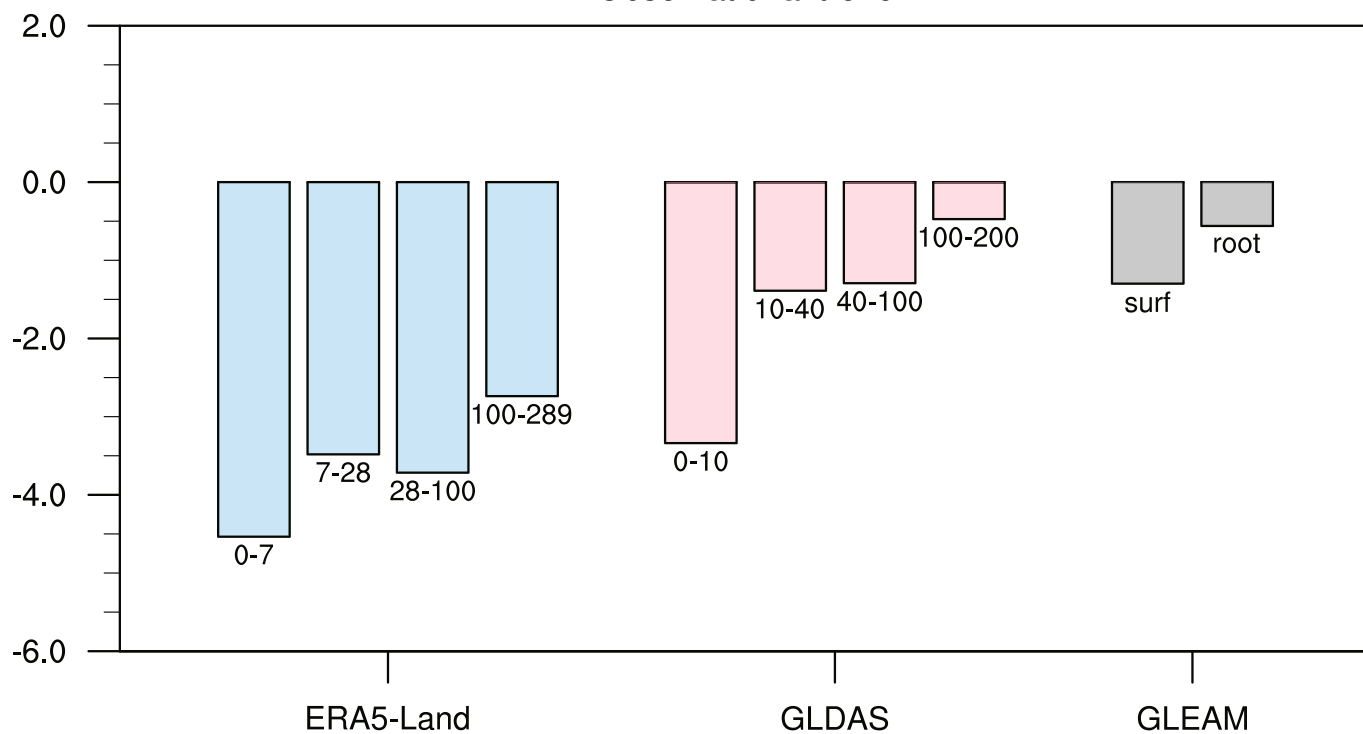


Extended Data Fig. 5 | The impact of precipitation and surface air temperature on surface soil moisture content. **a–d**, Mean anomalies of AMJ surface soil moisture content (%) for each percentile bin of MAM precipitation and AMJ surface air temperature during 1950–2020 derived from HadEX3,

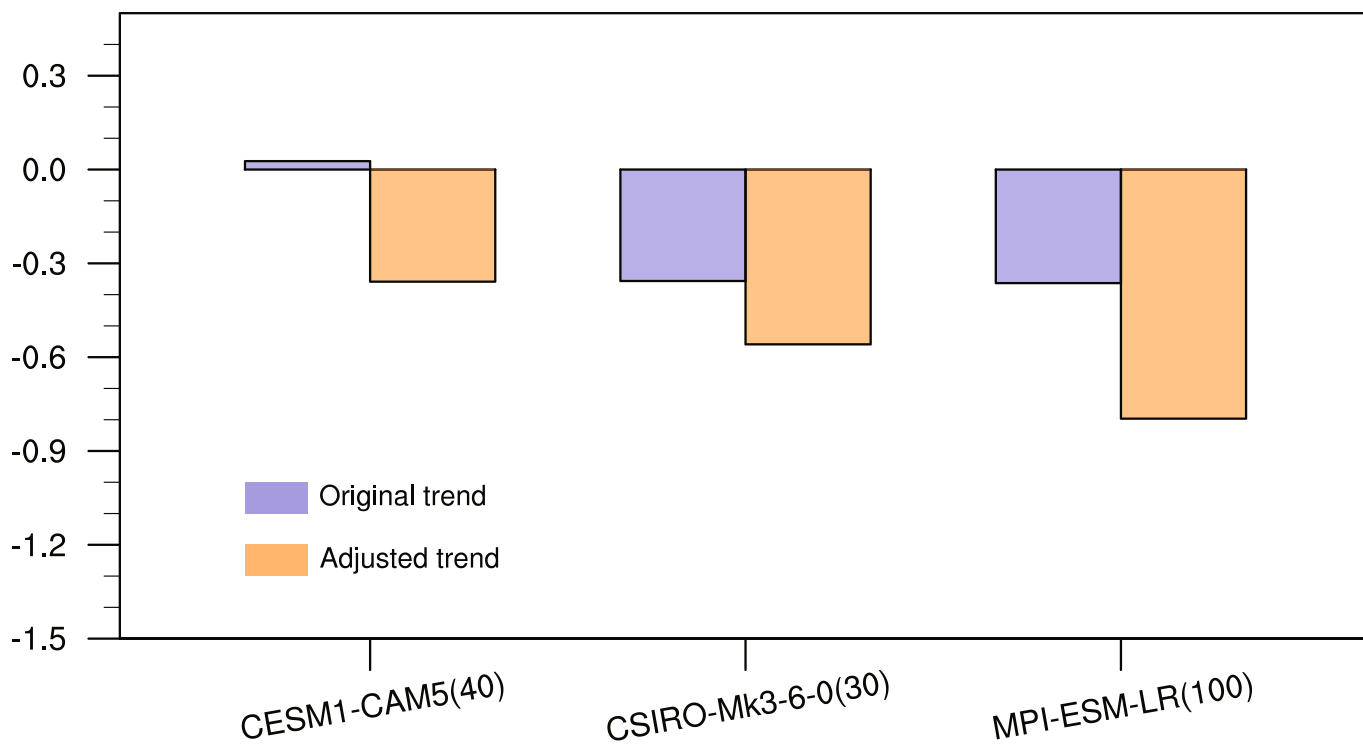
BEST, ERA5-Land (**a**), CESM1-CAM5 (**b**), CSIRO-Mk3-6-0 (**c**) and MPI-ESM-LR (**d**). Monthly values are used in (**a**) to enlarge the sample size, and all members are used in (**b–d**).

a

Observational trend

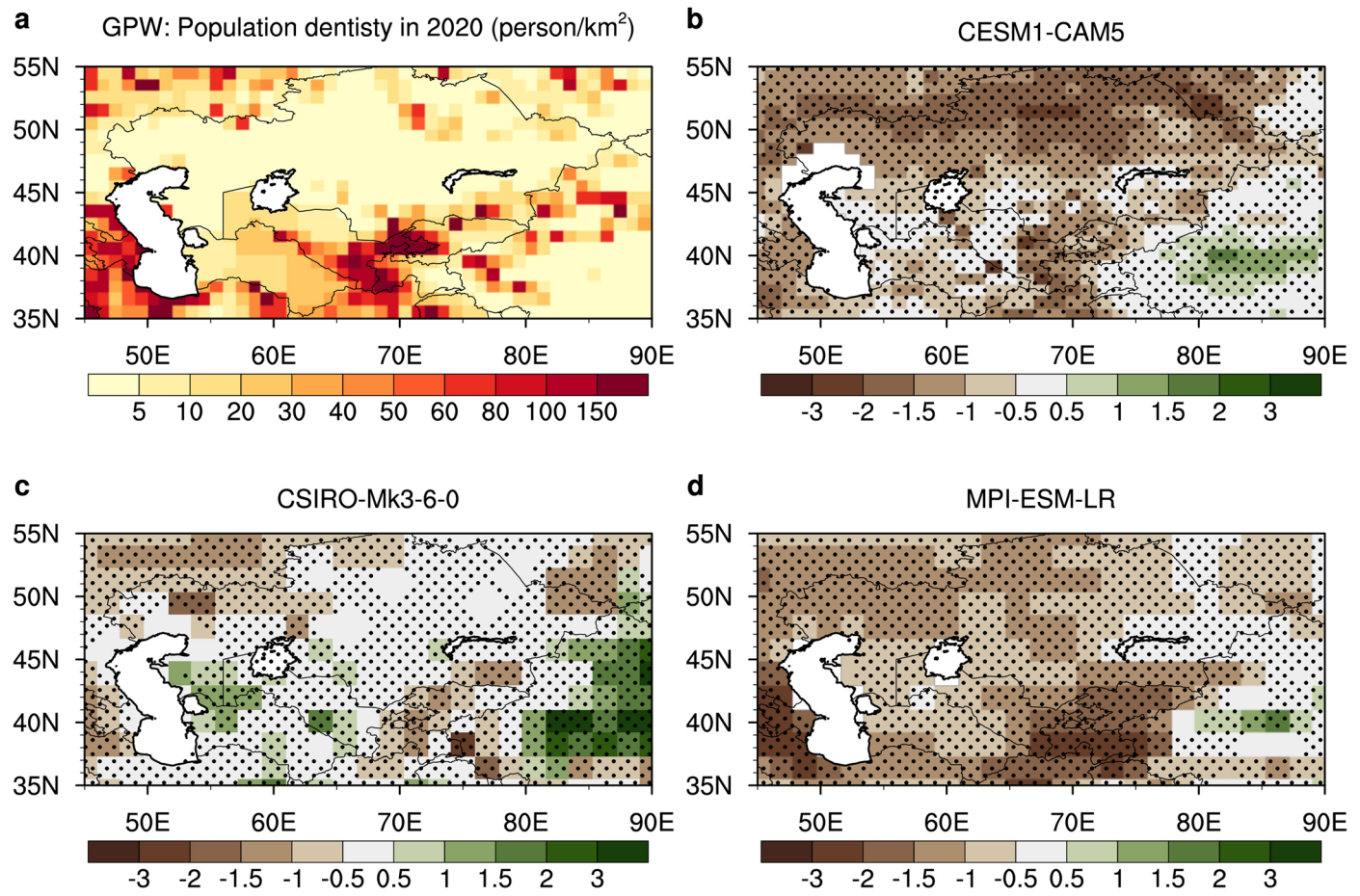
**b**

Simulated trend



Extended Data Fig. 6 | The changes in AMJ soil moisture content at different soil layers over southern Central Asia during 1992–2020. **a**, The trends in AMJ soil moisture content at different soil layers (%/decade) during 1992–2020 over southern Central Asia obtained from ERA5-Land (blue; 0–7, 7–28, 28–100 and

100–289 cm), GLDAS (ended 2014, pink; 0–10, 10–40, 40–100 and 100–200 cm) and GLEAM (grey; surface and root-zone). **b**, The original (blue) and adjusted trends (orange) in AMJ total soil moisture content during 1992–2020 obtained from CESM1-CAM5, CSIRO-Mk3-6-0 and MPI-ESM-LR, respectively.



Extended Data Fig. 7 | Future changes in AMJ surface soil moisture content over Central Asia. **a**, Population density in 2020 derived from GPW V4. **b–d**, Long-term changes in AMJ surface soil moisture content (%/decade) during 2021–

2099 derived from the ensemble mean of CESM1-CAM5 (**b**), CSIRO-Mk3-6-0 (**c**) and MPI-ESM-LR (**d**). Stippling indicates that the linear trends are significant at the 10% level according to the MK test.

Extended Data Table. 1 | Observed and simulated trends in surface soil moisture content over southern Central Asia

Data/Model	P1 (1950-1992)			P2 (1992-2020)		
	EM	IPO-induced	Adjusted	EM	IPO-induced	Adjusted
GLDAS (ended 2014)	-0.10			-3.34**		
ERA5-Land	1.35**			-4.53**		
GLEAM	—			-1.29		
ESACCI	—			-2.12**		
CESM1-CAM5	-0.07*	0.55 [0.10, 1.16]	0.48 [0.04, 1.09]	-0.08	-1.00 [-1.43, -0.43]	-1.08 [-1.51, -0.51]
CSIRO-Mk3-6-0	-0.23**	0.22 [-0.17, 0.58]	-0.01 [-0.40, 0.36]	-0.60**	-0.61 [-1.41, 0.43]	-1.21 [-2.01, -0.17]
MPI-ESM-LR	-0.40**	0.35 [-0.61, 1.16]	-0.05 [-1.01, 0.76]	-0.65**	-0.68 [-2.07, 0.86]	-1.34 [-2.72, 0.21]

The trends in surface soil moisture content (%/decade) over southern Central Asia in P1 (1950–1992) and P2 (1992–2020). The numbers in brackets denote the interquartile range (25–75%) among all members. For trends without interquartile range, ** denotes the trend significant at the 99% confidence level ($p < 0.01$); * denotes trend significant at the 95% confidence level ($p < 0.05$). EM: the trend for the ensemble mean; IPO-induced: the trend induced by the observational IPO evolution; Adjusted: the trend after adjustment.